

Antihydrogen annihilation reconstruction with the ALPHA silicon detector

G.B. Andresen^a, M.D. Ashkezari^b, W. Bertsche^c, P.D. Bowe^a, E. Butler^d, C.L. Cesar^e, S. Chapman^f, M. Charlton^c, A. Deller^c, S. Eriksson^c, J. Fajans^f, T. Friesen^g, M.C. Fujiwara^{h,g}, D.R. Gill^h, A. Gutierrezⁱ, J.S. Hangst^a, W.N. Hardyⁱ, M.E. Hayden^b, R.S. Hayano^j, A.J. Humphries^c, R. Hydomako^g, S. Jonsell^{c,k}, L.V. Jørgensen^c, L. Kurchaninov^h, N. Madsen^c, S. Menary^l, P. Nolan^m, K. Olchanski^h, A. Olin^h, A. Povilus^f, P. Pusa^m, E. Saridⁿ, S. Seif el Nasr^{i,1}, D.M. Silveira^o, C. So^f, J.W. Storey^{h,2}, R.I. Thompson^g, D.P. van der Werf^c, Y. Yamazaki^{o,p}, ALPHA Collaboration*

^a Department of Physics and Astronomy, Aarhus University, DK-8000 Aarhus C, Denmark

^b Department of Physics, Simon Fraser University, Burnaby, BC, Canada V5A 1S6

^c Department of Physics, Swansea University, Swansea SA2 8PP, UK

^d European Laboratory for Particle Physics, CERN, CH-1211 Geneva 23, Switzerland

^e Instituto de Física, Universidade Federal do Rio de Janeiro, Rio de Janeiro 21941-972, Brazil

^f Department of Physics, University of California, Berkeley, CA 94720-7300, USA

^g Department of Physics and Astronomy, University of Calgary, Calgary, AB, Canada T2N 1N4

^h TRIUMF, 4004 Wesbrook Mall, Vancouver, BC, Canada V6T 2A3

ⁱ Department of Physics and Astronomy, University of British Columbia, Vancouver, BC, Canada V6T 1Z4

^j Department of Physics, University of Tokyo, Tokyo 113-0033, Japan

^k Department of Physics, Stockholm University, SE-10691 Stockholm, Sweden

^l Department of Physics and Astronomy, York University, Toronto, ON, Canada M3J 1P3

^m Department of Physics, University of Liverpool, Liverpool L69 7ZE, UK

ⁿ Department of Physics, NRCN-Nuclear Research Center Negev, Beer Sheva IL-84190, Israel

^o Atomic Physics Laboratory, RIKEN, Saitama 351-0198, Japan

^p Graduate School of Arts and Sciences, University of Tokyo, Tokyo 153-8902, Japan

ARTICLE INFO

Article history:

Received 14 July 2011

Received in revised form

27 April 2012

Accepted 27 April 2012

Available online 6 May 2012

Keywords:

Antihydrogen

Antimatter

Event reconstruction

Vertexing detector

Cosmic ray background suppression

ABSTRACT

The ALPHA experiment has succeeded in trapping antihydrogen, a major milestone on the road to spectroscopic comparisons of antihydrogen with hydrogen. An annihilation vertex detector, which determines the time and position of antiproton annihilations, has been central to this achievement. This detector, an array of double-sided silicon microstrip detector modules arranged in three concentric cylindrical tiers, is sensitive to the passage of charged particles resulting from antiproton annihilation. This article describes the method used to reconstruct the annihilation location and to distinguish the annihilation signal from the cosmic ray background. Recent experimental results using this detector are outlined.

© 2012 Published by Elsevier B.V.

1. Introduction

The ALPHA experiment is engaged in the production and magnetic confinement of antihydrogen atoms [1,2]. With the apparatus located at the Antiproton Decelerator facility (AD) at CERN [3], the ALPHA collaboration intends to perform precision spectroscopic measurements on trapped antihydrogen [4] as a stringent test of CPT symmetry.

As with several other AD experiments [5–7], ALPHA synthesizes antihydrogen atoms by merging positron and antiproton

* Comments to the authors can be directed to alpha-contact@cern.ch.

¹ Present address: European Laboratory for Particle Physics, CERN, CH-1211 Geneva 23, Switzerland.

² Present address: Physik-Institut, Zürich University, CH-8057 Zürich, Switzerland.

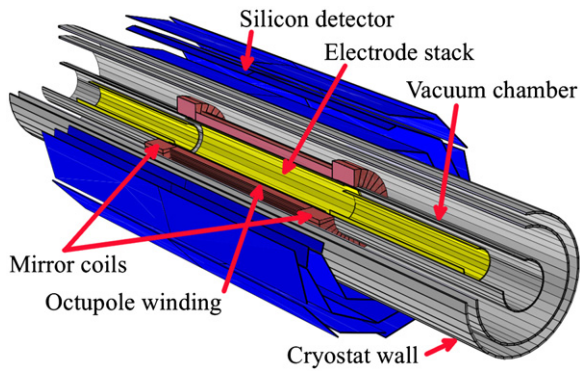


Fig. 1. Cut-away diagram of the antihydrogen production and trapping region of the ALPHA apparatus, showing the relative locations of the Penning-Malmberg trap (the external solenoid providing the axial magnetic field is not shown), neutral-atom trap magnets, and silicon detector.

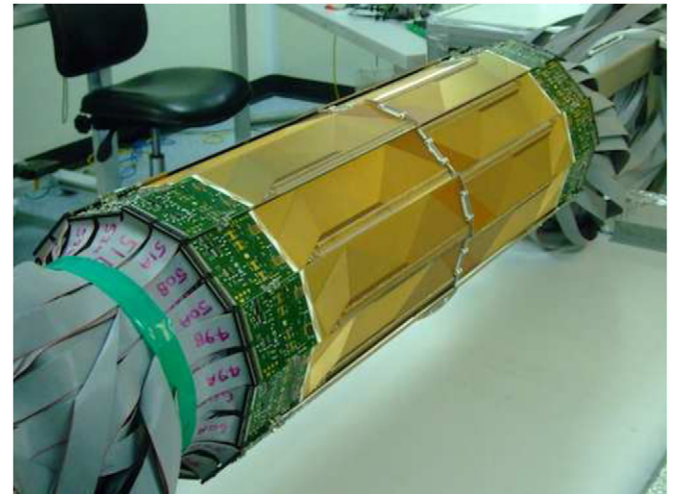


Fig. 2. The ALPHA Silicon Detector during construction at the University of Liverpool. The line segments within the gold rectangles are the leads connecting the microstrips to the readout electronics (the silicon wafers and microstrips are located on the opposite side of the modules and cannot be seen). The green rectangular sections contain the on-board readout electronics, and the grey cables carry the analog and digital signals to the rest of the readout system. (For interpretation of the references to color in this figure caption, the reader is referred to the web version of this article.)

plasmas [8,9], which themselves are contained in a Penning-Malmberg charged particle trap (Fig. 1). However, without additional confining potentials, the electrically neutral antihydrogen atoms escape the fields used to confine and manipulate the charged antiparticles. To prevent some of the newly formed antiatoms from traveling to the apparatus walls and annihilating, the ALPHA experiment employs a minimum-B neutral atom trap. This neutral trap consists of an array of superconducting magnets which provides a strong inhomogeneous magnetic field [10]. By exploiting the interaction between the magnetic moments of the atoms and the magnetic field gradient, very low energy ($< 50 \mu\text{eV}$), low-field seeking, antihydrogen atoms have been confined for as long as 1000 s [2].

To detect and locate annihilations, ALPHA has constructed a silicon tracking detector [11,12]. This detector is similar to that used in the ATHENA antihydrogen experiment [13–15], although the ALPHA instrument does not contain CsI crystals for γ -ray detection, and has three layers of modules to ATHENA's two (see Ref. [16] for design considerations of the ALPHA detector). The detection method is based on the reconstruction and extrapolation of the trajectories of charged annihilation products (primarily charged pions), which enables a 3-dimensional determination of the antiproton annihilation position, or 'vertex'.

The overarching design consideration for the ALPHA detector was to ensure compatibility with the rigid experimental requirements necessary for the magnetic trapping of antihydrogen. These constraints include the presence of a large amount of material between the annihilation point and the detector, as well as limited space available to house the detector. Despite these challenges, the annihilation detection and event reconstruction by this silicon detector provided a crucial tool for the unambiguous demonstration of antihydrogen trapping [1,2]. This article reports the details of the vertex reconstruction algorithm, as well as the analysis method for background suppression, used by the ALPHA experiment. The methods described here are an improved version of those used in Ref. [1] and were applied to the analysis of the data presented in Ref. [2].

2. The ALPHA detector and apparatus

The ALPHA detector (shown in Fig. 2) consists of 60 double-sided silicon microstrip modules arranged in three concentric layers. The detector is split axially into two sections, each containing 30 modules. Fig. 3 shows the configuration of the silicon modules and their locations with respect to the rest of the apparatus. The inner and middle layers are situated around the

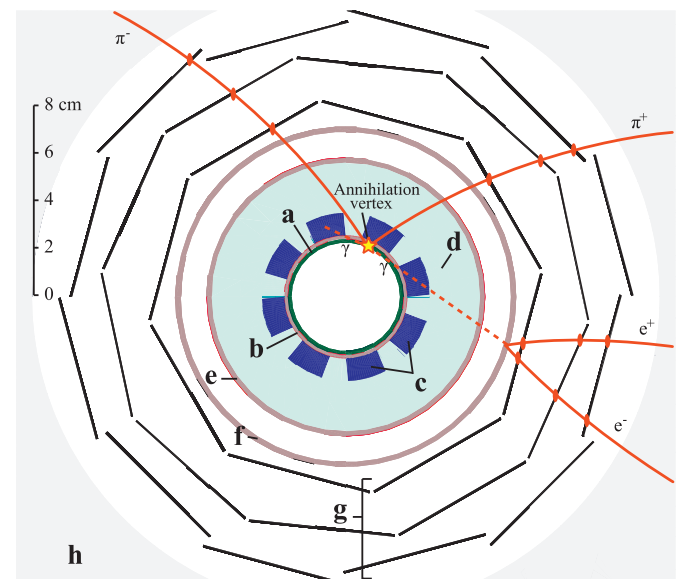


Fig. 3. Cross-sectional schematic of the axial center of the ALPHA apparatus and detector (to scale). The labeled apparatus elements are as follows: (a) electrode stack, (b) magnet winding form, (c) octupole magnet winding, (d) liquid helium volume, (e) inner isolation vacuum wall, (f) outer isolation vacuum wall, (g) silicon detector, and (h) external solenoid magnet. The two mirror coils at the axial ends of the magnetic neutral atom trap are not shown. A cartoon illustration of an antiproton annihilation resulting in three pions (two charged and one neutral) is also shown, where the annihilation vertex is given as the yellow star. The curves represent the trajectories of the annihilation products, with the ovals indicating where the particles passed through a silicon module. The neutral pion has quickly decayed through the $\pi^0 \rightarrow 2\gamma$ channel. One of the resulting photons has its energy attenuated and is finally absorbed in the octupole winding, while the other photon produced an electron–positron pair. (For interpretation of the references to color in this figure caption, the reader is referred to the web version of this article.)

trap axis with radii of 7.5 cm and 9.55 cm, respectively, while the outer layer is split between radii of 10.9 cm and 11.4 cm.

Each detector module has an active silicon area of $6 \text{ cm} \times 23 \text{ cm}$, with 256 readout strips with a pitch width of $227 \mu\text{m}$ in the $R-\phi$ direction, and 256 readout strips with a pitch width of $875 \mu\text{m}$ in

the z direction (where R , ϕ , and z are cylindrical coordinates). Since the signal collection strips run in orthogonal directions on opposite sides of the silicon wafer, the point of intersection between the particle trajectory and the silicon module can be localized in the 3-dimensional reference frame of the detector (the point of intersection is normally called a ‘hit’). The total axial extent of the detector is 46 cm, which provides a solid angle coverage of $\sim 90\%$ for annihilations in the axial center.

For the purposes of this article, an ‘event’ refers to the full operation of triggering and digitization of all the signal strips. To coordinate the strip triggering and digitization, every detector module has four VAITA [17] Application Specific Integrated Circuits (ASIC), where each ASIC handles 128 strips. The analog strip signals from the ASIC readout chips are digitized by five 48-channel VME-based VF48 ADC modules [18]. The programmable trigger condition is set to readout the entire detector when two or more $R-\phi$ strips from the inner layer of the detector register signal. This trigger is deliberately intended to accept a broad category of events, as the number of trapped antihydrogen atoms is known to be small and it is important to accept as many of these rare events as possible. Through a dedicated cross-calibration with external scintillation detectors with overlapping solid angles, the overall trigger efficiency is estimated to be $(90 \pm 10)\%$.

In total, this detector contains 30,720 signal strips, of which 30,195 (or 98.3%) are fully functioning. The large majority (512 strips) of the absent signal strips are the result of a non-functioning and disconnected module. The functioning strips typically operate with a leakage current of < 8 nA per strip at room temperature. The peak readout rate for this detector is 500 events/s, where each readout event contains the analog signal output for every strip. The amplitude of the analog signal is proportional to the number of electron-hole pairs liberated during the passage of a particle through the silicon volume. A dynamic thresholding algorithm, which utilizes knowledge of the amount of baseline charge collected for each strip (i.e. the pedestal), is used, on an event-by-event basis, to determine which strips registered signal. To account for the possibility that the charge is shared over multiple strips, adjacent strips are grouped together and the cluster center is determined via the ‘center of gravity’ algorithm [19]. However, because of the large pitch width, the large majority (about 75%) of strips registering signal are unaccompanied by any adjacent signal strips. Thus, to a good approximation, the hit resolution is $227/\sqrt{12} = 65 \mu\text{m}$ in the $R-\phi$ direction, and $875/\sqrt{12} = 253 \mu\text{m}$ in the z direction.

When reconstructing the paths of charged particles passing through the detector, any materials or fields that might affect the particle trajectories must be taken into account. In the ALPHA apparatus, annihilation products must pass through an electrode stack, superconducting magnet windings, and vacuum chamber walls before reaching the detector (Fig. 3). Moreover, the trap electrodes and silicon detector are surrounded by an external solenoid magnet, which provides a strong axial magnetic field (typically 1 T). Charged particles with low transverse kinetic energy will gyrate around the axial magnetic field lines. Simultaneously, the electrode stack imposes an axial electric field. In addition to the Penning-Malmberg trap, a significant portion of the ALPHA apparatus is dedicated to the magnetic neutral trap. In order to provide the maximum radial field magnitude within the trap region, the superconducting octupolar magnet is located as close to the trap region as possible [10]. For this reason, the particles resulting from antiproton annihilation will travel through a large amount of scattering material before encountering the silicon detector. This will worsen the resolution of the calculated vertex position, as the reconstructed trajectories of scattered particles do not lead directly back to the annihilation position. Specifically, a charged particle traveling outward from

the center of the apparatus will encounter the equivalent of between 40% and 70% of a radiation length of material depending on the track angle, and whether the trajectory of the particle encounters the superconducting winding of the neutral atom trap. This scattering can cause the calculated particle trajectory to deviate from its actual trajectory by as much as several millimeters for an extrapolated track with path length of about 5–15 cm.

3. Annihilation position reconstruction

The ALPHA silicon detector event reconstruction algorithms attempt to determine the antiproton annihilation position within the ALPHA apparatus. This task is divided into two parts: (1) the identification and reconstruction of the trajectories (tracks) of the charged particles released during antiproton annihilation (track reconstruction), and (2) the determination of the primary annihilation position using the track information (vertex determination). Throughout the reconstruction process, knowledge of the detector geometry and the outgoing particles’ characteristics is exploited to optimize the overall procedure.

3.1. Track reconstruction

Low-energy antiproton annihilation produces a relatively small number of particles compared, for example, to a hadron collider environment. On average, an antiproton annihilation (either on the electrode surface or on residual gas atoms) produces about three charged pions and two neutral pions [20]. While charged pions are stable on the timescale required to reach the detector, neutral pions decay essentially instantly ($\sim 10^{-16}$ s) into γ -rays, which, in turn, will often produce e^-e^+ pairs when transiting the apparatus material (Fig. 3). It should also be noted that stopped antiprotons can also fragment gold nuclei residing on the electrode surface, resulting in residual product nuclei along with α , β , and γ -ray backgrounds [21]. However, due to the amount of apparatus material, very few massive fragmentation products will arrive at the detector. Likewise, a large fraction of the γ -ray background from nuclear fragmentation is attenuated by the material of the neutral-atom trap.

In the ALPHA detector, most events will have between 9 and 15 hits (where a ‘hit’ is the intersection of orthogonal strips, translated into the 3-dimensional reference frame of the detector, as discussed in Section 2). The small average number of hits per event allows for the full examination of all hit combinations, and in turn provides a significant advantage for track finding. For example, ‘ghost hit’ ambiguities (where two or more particles pass through a single detector module and the orthogonal strip geometry results in several false hits) are resolved in a straightforward way: track candidates containing ghost hits do not conform to a helical trajectory and do not survive the track selection criteria. In the same situation, there will also be a track candidate containing the ‘true’ hits, and this candidate will be much more likely to satisfy the track selection criteria.

The ALPHA detector is located outside the trap cryostat, and therefore outside of the scattering material and inhomogeneous magnetic field of the neutral-atom trap, but still within the strong axial magnetic field of the Penning-Malmberg trap. As such, the trajectories of the charged particles as they pass through the detector are, to a good approximation, helical. A Monte Carlo simulation was implemented using GEANT3 within the ROOT Virtual Monte Carlo software package [15,22–24] with a realistic magnetic field map generated with the TOSCA/OPERA3D field solver package [25]. This simulation allowed for the study of the passage of charged particles through the apparatus material and

field. Apart from deviations due to multiple scattering, the simulated charged particles indeed follow helical trajectories in the homogeneous region of the field containing the silicon detector.

Tracks recorded by the ALPHA detector are predominately attributed to charged pions produced during antiproton annihilation. The detector geometry allows each outgoing particle trajectory to be sampled a maximum of three times, regardless of track angle, which is sufficient to determine the track parameters needed to extrapolate the helical trajectory in the solenoidal magnetic field. For this reason, a track candidate in the ALPHA detector is defined as a collection of exactly three hits (one in each detector layer).

In order to identify the charged tracks in an event, every possible three-hit combination is examined. Each track candidate has six hit degrees of freedom—that is, each of the three hits has two degrees of freedom in the directions perpendicular to that of the strips. After determining the five helix parameters, each track is left with only one effective degree of freedom, which contributes only in the axial projection of the track. Track candidates can then be selected based, in part, on how closely the candidates conform to helical trajectories in the axial projection. Specifically, a χ^2 figure of merit can be constructed which compares the positions where the determined helix trajectory intersects the silicon detector modules to the measured hit positions. However, since only three hits are available for each track candidate, the helix parameters in the plane perpendicular to the magnetic field are exactly determined. Thus, for the plane perpendicular to the magnetic field, the computed trajectories always pass exactly through the hit locations such that these terms do not contribute to the χ^2 measure. As such, the χ^2 figure of merit reflects only how well the track candidates conform to a helical trajectory in the axial projection, and only candidates for which $\chi^2 < 5$ are considered for the vertex reconstruction. Additionally, track candidates are rejected if their reconstructed trajectories do not pass within a radius of 3.73 cm from the trap axis (which corresponds to a volume extending from the trap axis out to a radius 1.5 cm beyond the inner surface of the Penning-Malmberg trap electrodes).

It should also be stressed that since the helix parameters in the plane perpendicular to the magnetic field are exactly determined, the track covariance matrix cannot be fully populated. That is, there is no measure of uncertainty for the radial trajectory of the track candidates. As a result, without full covariance matrices, sophisticated vertex determination methods (i.e. least-squares fitting or Kalman filter methods) are precluded.

The track finding efficiency of this algorithm is evaluated using the Monte Carlo simulation described above. After all the track selection criteria are applied, the track finding efficiency of this algorithm is found to be $(88 \pm 5)\%$ for all charged tracks (regardless of particle species) with three hits. This highlights the advantage of evaluating every hit combination, as only a small number of tracks are missed due to atypical trajectories through the detector modules, often because of particle scattering within the silicon itself. However, many of these properly determined tracks are due to e^-e^+ pairs. As such, although they return acceptable tracks, these tracks are not guaranteed to extrapolate back to the annihilation vertex.

3.2. Vertex reconstruction

An annihilation vertex is defined to be a convergence of particle tracks. In order to locate such vertices, the particle tracks identified in Section 3.1 are extrapolated into the trapping region near the radial center of the ALPHA apparatus (Fig. 3). Track extrapolation covers a path length of at least 5.3 cm, and as much

as ~ 14 cm, where the particle trajectory will necessarily have passed through several layers of scattering material. The annihilation vertex is taken as the point where the tracks pass closest to each other. The effect of the scattering material is to increase the statistical variance of the vertex position determination.

The measured vertex position, $\mathbf{r}_{\text{vertex}}$, is determined through the minimization of a figure of merit, D , which represents the mean distance of closest approach of the tracks to the vertex position:

$$D = \frac{1}{N_{\text{tracks}}} \sum_{i=1}^{N_{\text{tracks}}} d_i \quad (1)$$

where N_{tracks} is the number of tracks used in the vertex determination, and d_i is the distance of closest approach of the i -th track, with track position \mathbf{r}_i , to the vertex position:

$$d_i^2 = \min\{|\mathbf{r}_i - \mathbf{r}_{\text{vertex}}|^2\}. \quad (2)$$

The minimization of Eq. (1) will then return a vertex position which balances the contributions from all the included tracks. Each track is treated equally in this procedure, regardless of its dip-angle or the material it encounters along its trajectory. As such, it is preferable to include as many tracks as possible, as each track will constrain the position of the vertex. However, it is important to exclude tracks which do not converge with their counterparts, as these tracks can bias the vertex reconstruction away from the true annihilation position.

The track exclusion algorithm proceeds as follows:

1. Do not proceed if $N_{\text{tracks}} \leq 2$, as at least two tracks are needed to form a vertex.
2. Reconstruct the vertex position using all the available tracks and calculate the mean distance of closest approach for this initial configuration, D_0 . Additionally, construct N auxiliary vertices, where each new vertex configuration excludes a different track (all the new vertices will therefore include $N_{\text{tracks}} - 1$ tracks).
3. Calculate the mean distance of closest approach for each new vertex configuration. Determine which track configuration has the smallest mean distance of closest approach, and call this value D_{min} .
4. Calculate $\Delta D = (D_0 - D_{\text{min}})/D_0$, which gives the fractional improvement in the mean distance of closest approach by excluding that specific track from the vertex.
5. If $\Delta D \leq D_{\text{cutoff}}$, exit the algorithm, keeping the configuration associated with D_0 as the final vertex determination. D_{cutoff} sets the threshold on the fractional change in D . For the ALPHA detector, a cutoff of $D_{\text{cutoff}} = 0.4$ was determined by optimizing the effect of this threshold on the vertex resolution using results from the Monte Carlo simulation of our system.
6. If $\Delta D > D_{\text{cutoff}}$, the configuration of tracks associated with D_{min} is promoted to the current accepted configuration, and relabeled as D_0 for the remainder of the algorithm.
7. If the track configuration now associated with D_0 has more than two tracks, return to Step 2 with this configuration.

Fig. 4(a) shows an example event after the entire reconstruction procedure, including track exclusion. In this example, four tracks were identified, but the three solid curves show the tracks that returned the best determination of the vertex position. The resolution of the vertex determination can then be estimated using the Monte Carlo simulation of the antiproton annihilation on the electrode surface. Because the simulated annihilation position is known, the reconstructed position uncertainty can be evaluated, as shown in Fig. 5. Here, the distribution of differences between the simulated and reconstructed positions is fitted with

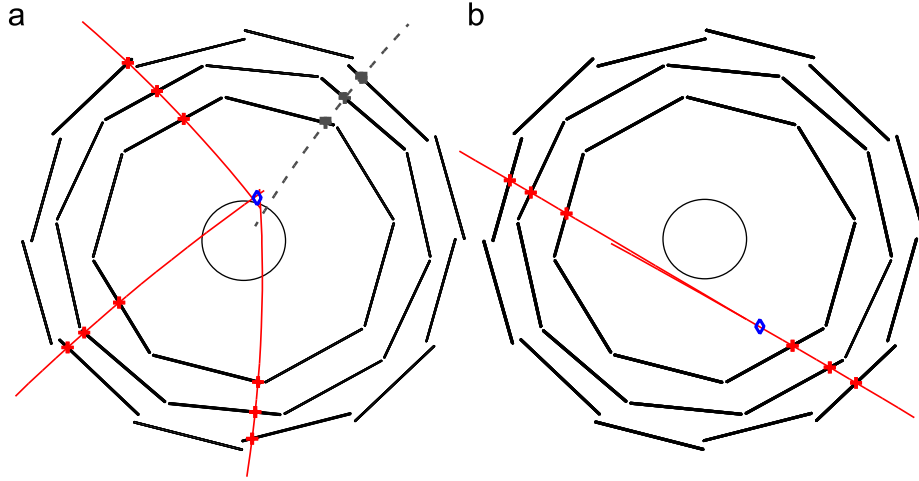


Fig. 4. Example reconstruction of (a) an annihilation event and (b) a cosmic background event. The crosses indicate hits registered in the silicon microstrip modules, while the solid curves show the reconstructed particle tracks. The dashed track illustrates a track that was considered, but ultimately excluded from the vertex determination. The reconstructed vertex is shown as the hollow diamond.

a resolution function comprised two independent Gaussian terms, whose fitting parameters are given in Table 1. With this resolution function, the narrow Gaussian term represents well-reconstructed vertices, while the broad Gaussian term includes events where the vertex is poorly reconstructed, usually resulting from the inclusion of inappropriate, or inadequately measured, tracks. It is also useful to consider an effective resolution which characterizes the full distribution. As such, the full width at half maximum (FWHM) is used to provide a measure of the overall uncertainty in the reconstructed vertex position. The effective axial resolution is found to be 0.56 cm, while the resolution in the radial component of the vertex position is found to be 0.87 cm, and the azimuthal resolution is 21.4° (which, at the electrode radius of 2.2275 cm, corresponds to 0.83 cm FWHM).

4. Cosmic background rejection

In addition to charged annihilation products, the ALPHA detector is also sensitive to the passage of charged particles originating from cosmic rays (Fig. 4b shows an example cosmic ray event). It is important to reduce the cosmic ray background in order to assist the identification of antihydrogen annihilations, especially for the observation of magnetically trapped antihydrogen. The large majority of cosmic background events are identifiably different from annihilation events and can be rejected event-by-event.

4.1. Discriminating variables

Cosmic rays that graze the detector do not typically produce a vertex and are automatically rejected. A vertex is often reconstructed, however, when the cosmic ray particle passes through the center of the detector. Fortunately, the distinct topologies of annihilation and cosmic ray events can be used to classify events as signal (annihilation, e.g. Fig. 4a) or background (cosmics, e.g. Fig. 4b). There are several variables that can be used to quantify the different signal and background topology: the number of charged tracks, N_{tracks} ; the combined linear fit residual, δ ; and the vertex radial position, R .

4.1.1. Number of charged tracks, N_{tracks}

The majority of cosmic background events which return a vertex position contain two charged tracks ($N_{\text{tracks}} = 2$), according

to our definition that tracks must contain exactly three hits, with one hit in each detector layer. This follows from the fact that these events are generally produced by the passage of a single charged particle, such that the two tracks found in the event are just segments of a single charged track.

Conversely, the average charged multiplicity from antiproton annihilation results in roughly three charged tracks per annihilation. This means that a large number of annihilation events (about $\sim 46\%$ of reconstructed vertices) will contain more than two charged tracks ($N_{\text{tracks}} > 2$). However, there is still substantial overlap between the signal and background N_{tracks} distributions, wherein many annihilation events contain only two charged tracks, while some cosmic background events are accompanied by particle showers or scattering resulting in large numbers of tracks in those events.

4.1.2. Combined linear fit residual, δ

Cosmic ray particles passing through the ALPHA detector are expected to follow, to first order, straight-line trajectories. Thus, events consistent with a single, linear, particle track are likely to be the result of the passage of a cosmic particle. To test for this case, the hit positions in an event can be fitted with a line. The combined linear residual, δ , can be used to evaluate how closely an event conforms to a single straight line track. This estimator is written as

$$\delta = \min \left\{ \sum_{i \in \mathcal{F}} d_{\perp,i}^2 \right\} \quad (3)$$

where $d_{\perp,i}$ is the perpendicular distance, or residual, between the fitted line and the i -th hit in the set of hits, \mathcal{F} . Finally, the minimization of Eq. (3) involves iterating over every pair of tracks. This iteration is done to ensure that, even if the event contains several tracks, the combination providing the best fit, or smallest value for δ , is chosen. The track pair with the smallest δ is used to characterize the event, as this analysis is explicitly intended to identify cosmic-like events.

If the hits in an event fit a perfect line, δ will evaluate to zero. However, due to their curvature in the magnetic field and multiple scattering as they pass through the apparatus and detector, cosmic trajectories often deviate from the ideal, resulting in a broadening of the δ distribution. Annihilation events, on the other hand, are not expected to produce many co-linear tracks, and should return values of δ well removed from the cosmic

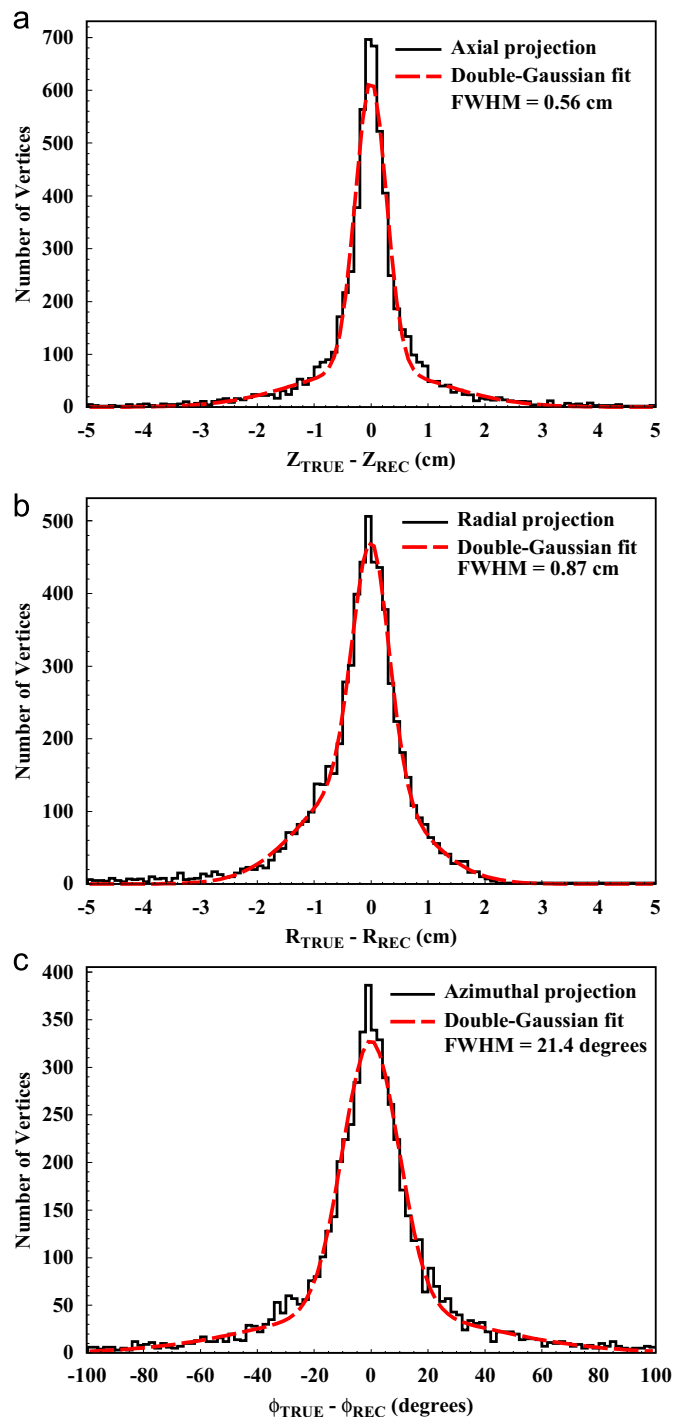


Fig. 5. The distributions of differences between true and reconstructed positions for simulated annihilation vertices for the (a) axial, (b) radial, and (c) azimuthal coordinates. The dashed line shows the result of fitting a function with two independent Gaussian terms (denoted broad and narrow), with the fitting parameters given in Table 1.

distribution. The δ -cut is set to account for the curvature and multiple scattering of cosmic trajectories, while minimizing the loss of acceptance for annihilation events.

4.1.3. Vertex radius, R

Annihilations must originate from within the trapping region of the apparatus, either on the surface of the electrodes or on

background gas. This physical constraint restricts the possible locations of the reconstructed vertex. In particular, the radial coordinate of the annihilation vertex is expected to be, within the radial reconstruction resolution, at the electrode radius. Likewise, it is reasonable to assume that reconstructed vertices far outside the trap volume are spurious and unphysical.

A cosmic event with two co-linear tracks, however, will return a vertex that is unconstrained in the radial coordinate and often well outside the trapping volume (an example of such a vertex is Fig. 4b). Thus, events where the vertex radius is much greater than the electrode radius are attributed to cosmic rays and categorized as background.

4.2. Datasets

Representative sample sets are required for both the annihilation signal and cosmic background in order to place the cuts on the discriminating variables. In the case of the ALPHA experiment, the signal and background can be measured separately, and as such, dedicated data samples can be collected for each.

The annihilation signal sample was constructed from 335 cycles where positrons and antiprotons were mixed together to form antihydrogen in the magnetic field of the neutral atom trap [9]. Each mixing cycle lasted for 1 s, and a total of 165,520 readout events were collected. Over the combined 335 s of signal collection, about 3350 events are expected from cosmic background, which constitutes a contamination of $\sim 2\%$.

Conversely, the background sample set was collected by operating the detector with no antiparticles present within the apparatus. So as to best emulate the situation of interest, the neutral trap magnets were kept engaged throughout the background collection. Data were recorded over several periods, which totaled almost 3 h, with 109,824 readout events. With no antiparticles present, these events should all be background signals, from such sources as cosmic or electronic noise-induced detections.

4.3. Cut placement and optimization

The separation of signal from background is only effective with well placed cuts on the discriminating variables. These cuts are determined so as to maximize the number of cosmic events rejected, while retaining as many annihilation events as possible. This analysis is focused on optimizing the expected signal significance during attempts to trap antihydrogen. An appropriate figure of merit for this optimization is the p -value for a Poisson distribution, α . This p -value represents the probability of observing n_0 events (or more) solely due to a fluctuation in a Poisson-distributed background with mean b . Here, the expected signal and expected background can be parametrized as functions of cuts on the combined linear residual, δ_{cut} , and vertex radius, R_{cut} , as well as categorized according to the number of charged tracks, N_{tracks} , found in the event. The p -value figure of merit can then be written as

$$\alpha(n_0, b) = \sum_{n=n_0}^{\infty} \frac{b^n e^{-b}}{n!}, \quad (4)$$

where the observed events and background rate depend on the cuts used ($n_0 = n_0(R_{\text{cut}}, \delta_{\text{cut}}, N_{\text{tracks}})$ and $b = b(R_{\text{cut}}, \delta_{\text{cut}}, N_{\text{tracks}})$). The signal optimization then proceeds by finding the set of cuts which minimize $\alpha(n_0, b)$, or equivalently, maximize the signal significance. In order to avoid unintentional bias, all analyses were performed and finalized on the auxiliary datasets described in Section 4.2. Moreover, the cut optimization was performed blindly, i.e. without direct reference to the trapping data.

Table 1
Table of fitting parameters for the double-Gaussian resolution functions shown in Fig. 5.

Coordinate	Axial	Radial	Azimuthal
<i>Narrow Gaussian term</i>			
Area	373 ± 10	268 ± 17	7050 ± 210
Mean	-0.004 ± 0.005 cm	-0.004 ± 0.010 cm	$-0.11 \pm 0.21^\circ$
Width	0.27 ± 0.01 cm	0.32 ± 0.02 cm	$9.9 \pm 0.3^\circ$
<i>Broad Gaussian term</i>			
Area	228 ± 9	344 ± 17	4240 ± 190
Mean	-0.04 ± 0.03 cm	-0.22 ± 0.02 cm	$0.52 \pm 0.93^\circ$
Width	1.29 ± 0.05 cm	0.99 ± 0.03 cm	$39.4 \pm 1.5^\circ$

The events are first separated into two categories: those with two charged tracks ($N_{\text{tracks}} = 2$) and events with more than two charged tracks ($N_{\text{tracks}} > 2$). This categorization separates the events into background-dominated, and signal-dominated sets, as the vast majority of background events fall into the $N_{\text{tracks}} = 2$ category (see Fig. 4(b) for an example of a typical background event). The $N_{\text{tracks}} > 2$ set then contains mostly signal events, with some background events to be rejected, while the $N_{\text{tracks}} = 2$ category contains primarily background events, with some signal events to be extracted. Thus, cuts on the $N_{\text{tracks}} = 2$ events should be relatively stringent to reject as many background events as possible, while the $N_{\text{tracks}} > 2$ cuts should be much more inclusive.

In order to optimize the expected signal significance, Eq. (4) is estimated over a wide range of radius and residual cuts, as well as for both N_{tracks} categories. Since b and n_0 are functions of the applied cuts, both parameters must be determined for every set of cuts. The background rate can easily be determined by directly applying the cuts to the cosmic background dataset and examining the surviving distribution. This method has the advantage of an accurate cosmic background estimate, since a direct measurement can be made. However, it is difficult to estimate the expected signal rate, as the dynamics of the antihydrogen distribution are not well characterized throughout the trapping experiments. Instead, a baseline number of signal events is taken from Ref. [28] and the expected number of events is determined for each set of cuts by scaling the baseline value according to the auxiliary annihilation distribution.

For a low-rate process such as antihydrogen trapping, n_0 is assumed to follow Poisson statistics. To reflect these statistics, an aggregate value for α is calculated (for each set of cuts) using 5000 pseudo-experiments. Each pseudo-experiment is performed as follows:

1. A Poisson distribution with mean n_0 is sampled so as to obtain an pseudo-experimental number of observed events, n_s .
2. The p -value for the pseudo-experiment is calculated $\alpha_i = \sum_{n=n_s}^{\infty} b^n \exp(-b)/n$.
3. The representative value for the ensemble of p -values is taken as the log-average $\alpha = \exp(1/n \sum_{i=1}^n \ln \alpha_i)$. This measure of central tendency takes into account the logarithmic nature of the distribution of pseudo-experimental p -values.

Fig. 6 shows the parameter space of the figure of merit as a function of the discriminating variables. The p -value is expressed in terms of standard deviations for a one-sided normal distribution, such that maximizing the expected significance corresponds to minimizing the expected p -value. These distributions are constructed by considering an array of $(R_{\text{cut}}, \delta_{\text{cut}})$ cut value pairs. The final set of cuts were then chosen so as to take into account the expected significance, and the final choices of cuts are shown as the black crosses in Fig. 6, and enumerated in Table 2. The

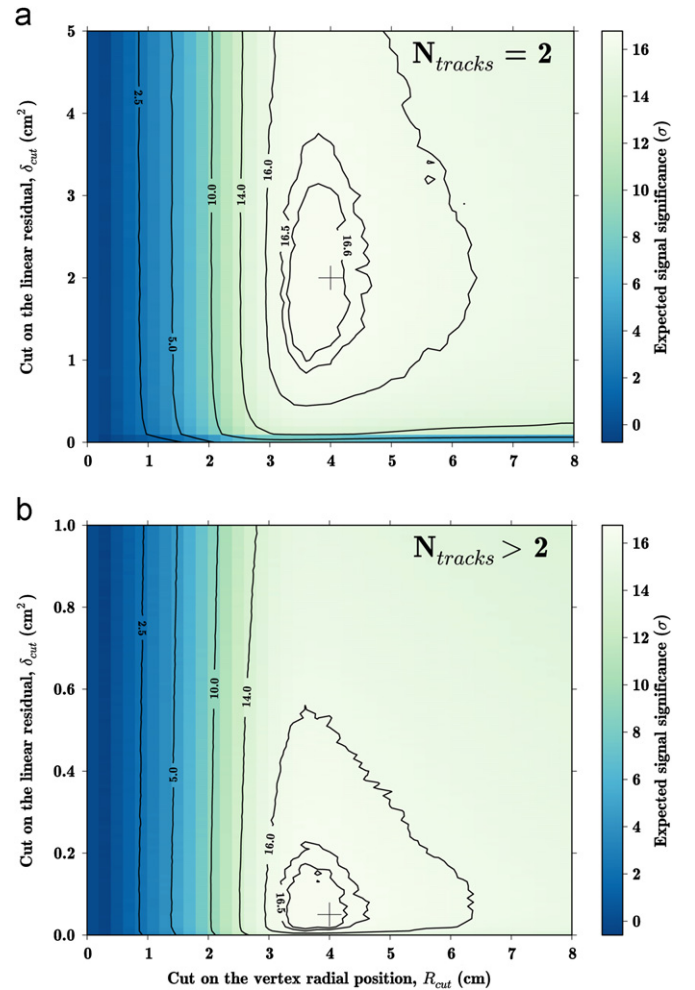


Fig. 6. Contour plots for the expected signal significance as a function of the cuts on the vertex radius, R_{cut} , and combined linear residual, δ_{cut} , for (a) events with $N_{\text{tracks}} = 2$ and (b) events with $N_{\text{tracks}} > 2$. The final cut decisions are shown as the black crosses.

Table 2
Final parameter cut conditions. Events satisfying these conditions are classified as annihilations.

N_{tracks}	Vertex radius, R_{cut} (cm)	Linear residual, δ_{cut} (cm^2)
$= 2$	< 4	> 2
> 2	< 4	> 0.05

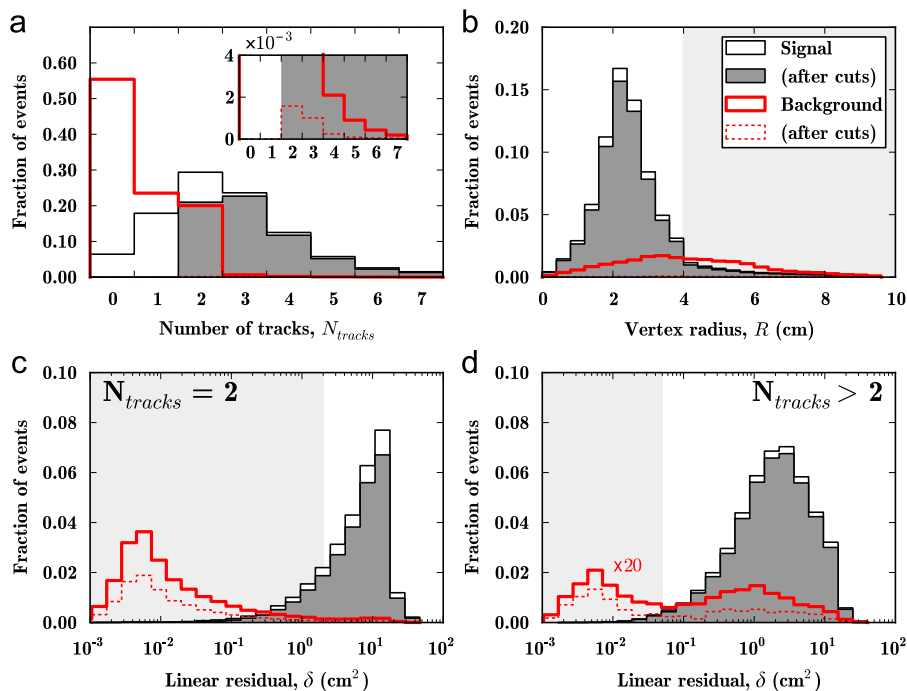


Fig. 7. Measured signal and background distributions for the discriminating variables. Shown are (a) the distribution of the number of charged tracks per event, N_{tracks} , (b) the radial component of the reconstructed vertex, R , and the combined linear residuals for the cases where (c) $N_{tracks} = 2$, and (d) $N_{tracks} > 2$. The annihilation signal sample is shown as the solid black trace, while the signal sample after the application of all other cuts than the one plotted is shown as the solid grey filled trace. The cosmic background sample is shown as the solid thick trace, and the dashed trace shows the background sample after the application of all other cuts than the one plotted. All distributions are normalized to the number of events in each sample set. The inset in (a) shows a magnification of the y-axis, highlighting the effect of the cuts on the background sample. Likewise, both background traces have been multiplied by a factor of 20 in (d) to allow for comparison. The lightly shaded areas represent the regions rejected by the cuts.

optimal placement of the cut values is unaffected when the estimated signal rate is varied, indicating that this analysis provides a robust determination of background rejection cuts.

4.4. Results of the background rejection

The effectiveness of the cut placement optimization can be evaluated by applying these cuts to the datasets described in Section 4.2. Fig. 7 shows the distributions of the discriminating variables for both signal and background datasets, along with the distributions after the application of the cuts. By applying the cuts to the background sample, $(99.54 \pm 0.02)\%$ of the events are rejected, corresponding to a background acceptance rate of $(47 \pm 2) \times 10^{-3}$ events/s.

Similarly, $(75.7 \pm 0.1)\%$ of events in the signal sample return a vertex and $(85.1 \pm 0.1)\%$ of those vertices survive the cuts, which combined give a signal acceptance of $(64.4 \pm 0.1)\%$. The overall detection efficiency is then $(58 \pm 7)\%$, which is the product of the trigger efficiency $(90 \pm 10)\%$ and the signal acceptance. Since the events included in these datasets were collected from *in situ* measurements (Section 4.2), the charge-collection and threshold efficiencies of the silicon modules are convolved into the above numbers.

5. Application to trapped antihydrogen detection

A strong motivation for the inclusion of a silicon detector in the ALPHA experiment is that it is sensitive to the annihilations of individual antiprotons. This is especially relevant for antihydrogen trapping experiments, where the expected number of trapped atoms is very small. During the 2009 experimental beamtime, 212 trapping experiments were completed, combining 10^7

antiprotons with 1.3×10^9 positrons [28]. Each trapping experiment involved the mixing of positrons and antiprotons to synthesize antihydrogen within the neutral atom trap fields, such that sufficiently low-energy antihydrogen atoms would be unable to escape the magnetic trap. Then, shortly after mixing was stopped, the neutral trap was quickly de-energized, allowing any trapped antihydrogen atoms to escape and annihilate. In total, 36 detector readout events were recorded in the 30 ms window during the fast shutdown of the neutral trap. After a blind analysis to determine the optimal cut placement (following Section 4), six events were identified that satisfied all selection criteria [28]. The cosmic ray event suppression provided a background acceptance rate of $(2.2 \pm 0.1) \times 10^{-2}$ events/s during these attempts (due to the specifics of the detector trigger used), the probability that all six events observed were due to statistical fluctuations in the cosmic ray background is 9.2×10^{-9} , corresponding to a signal significance of 5.6σ .

In addition to the cosmic ray particles, bare antiprotons that have been mirror-confined in the inhomogeneous magnetic field of the neutral-atom trap are another possible background [28]. Mirror-trapped antiprotons are a difficult background to isolate, as the annihilation signature of the bare antiproton is identical to that of released antihydrogen. However, mirror-trapped antiprotons can be ruled out as a source of annihilation signal by applying a static electric field during the shutdown of the magnetic trap. This bias field acts to axially deflect any charged particles, while leaving the neutral atoms unaffected [1]. This method of discriminating between released antihydrogen atoms and bare mirror-trapped antiprotons relies crucially on the axial reconstruction of the annihilation position. Specifically, while the release of trapped antihydrogen results in a vertex distribution that is axially extended across the length (14 cm) of the trap, mirror-trapped antiprotons will annihilate in an axially narrow

distribution [29]. Moreover, the applied bias field can be used to positively identify the presence of mirror-trapped antiprotons by shifting the average axial vertex position by as much as 14 cm, while leaving the distribution of antihydrogen vertices unchanged. The differences between these vertex distributions are readily observable, given the axial reconstruction resolution of 0.56 cm FWHM stated in Section 3.2.

During the 2010 AD beamtime, ALPHA performed 335 trapping experiments (similar to the experiments described above), combining a total of 10^7 antiprotons with 7×10^8 positrons. Crucially, almost a third of those trapping experiments involved the bias field to deflect any mirror-trapped antiprotons. Overall, 307 detector readout events were recorded during the 30 ms detection window, and 38 events satisfied all the annihilation selection criteria [1]. Moreover, the selected events formed an axial vertex distribution characteristic of released antihydrogen atoms, and inconsistent with bare mirror-trapped antiprotons. The confinement time during the initial trapping experiments was set to 172 ms, which was the shortest time required to perform the measurement. However, following refinements to the trapping procedure, the number of trapped atoms per attempt was increased by up to a factor of five and confinement times were lengthened to as long as 1000 s [2]. In total, 309 trapped antihydrogen annihilation events were recorded and examined during the 2010 experiments.

6. Summary

The ALPHA collaboration has constructed a silicon annihilation reconstruction detector for the purposes of detecting and studying antihydrogen. This article describes the methods related to the reconstruction of the vertex position of an antiproton annihilation. In addition, the analysis to optimize the background suppression is presented. After optimization, these algorithms permit a background rate of $(47 \pm 2) \times 10^{-3}$ events/s in the ALPHA detector, while accepting $(64.4 \pm 0.1)\%$ of the recorded annihilation events. The detector and methods described above were crucial to the successful observation of trapped antihydrogen, and will likely be an important part of future spectroscopic measurements in ALPHA.

Acknowledgments

This work was supported by CNPq, FINEP/RENAFAE (Brazil); ISF (Israel); MEXT (Japan); FNU (Denmark); VR (Sweden); NSERC, NRC/TRIUMF, AIF/AITF, FQRNT, and the Killam Trust (Canada); the DOE and the NSF (USA); and EPSRC, the Royal Society and the Leverhulme Trust (UK). We would like to thank D. Seddon, J. Thornhill, and D. Wells (University of Liverpool) for their work on the construction of the vertex detector.

References

- [1] G.B. Andresen, et al., *Nature* 468 (2010) 673.
- [2] G.B. Andresen, et al., *Nature Physics* 7 (2011) 558.
- [3] S. Maury, *Hyperfine Interactions* 109 (1997) 43.
- [4] C.L. Cesar, et al., *Canadian Journal of Physics* 87 (2009) 791.
- [5] M. Amoretti, et al., *Nature* 419 (2002) 456.
- [6] G. Gabrielse, et al., *Physical Review Letters* 89 (2002) 213401.
- [7] Y. Enomoto, et al., *Physical Review Letters* 105 (2010) 243401.
- [8] G.B. Andresen, et al., *Journal of Physics B: Atomic, Molecular and Optical Physics* 41 (2008) 011001.
- [9] G.B. Andresen, et al., *Physics Letters B* 685 (2010) 141.
- [10] W. Bertsche, et al., *Nuclear Instruments and Methods in Physics Research A* 566 (2006) 746.
- [11] M.C. Fujiwara, et al., *AIP Conference Proceedings* 1037 (2008) 208.
- [12] G.B. Andresen, et al., *Journal of Instrumentation* 7 (2012) C01051.
- [13] C. Regenfus, *Nuclear Instruments and Methods in Physics Research A* 501 (2003) 65.
- [14] M.C. Fujiwara, et al., *Physical Review Letters* 92 (2004) 065005.
- [15] M. Amoretti, et al., *Nuclear Instruments and Methods in Physics Research A* 518 (2004) 679.
- [16] M.C. Fujiwara, et al., *AIP Conference Proceedings* 793 (2005) 111.
- [17] VAITA Manual, Ideas ASA, Hovik, Norway.
- [18] J.-P. Martin, P.-A. Amaudruz, *IEEE Transactions on Nuclear Science NS-53* (2006) 715.
- [19] G. Landi, *Nuclear Instruments and Methods in Physics Research A* 485 (2002) 698.
- [20] G. Bendiscioli, D. Kharzeev, *Rivista del Nuovo Cimento* 17 (1994) 1.
- [21] P. Lubiński, et al., *Physical Review C* 66 (2002) 044616.
- [22] CERN Application Software Group, GEANT, CERN Program Library W5013, Geneva, 1993.
- [23] R. Brun, F. Rademakers, *Nuclear Instruments and Methods in Physics Research A* 389 (1997) 81.
- [24] I. Hřivnáčová, et al., arXiv:cs/0306005, 2003.
- [25] Commercial product from Vector Fields Software: (<http://www.vectorfields.com>).
- [26] G.B. Andresen, et al., *Physics Letters B* 695 (2011) 95.
- [27] C. Amole, et al., *New Journal of Physics* 14 (2012) 015010.